

Novel Dispersion of 1D Nanofiber Fillers for Fast Ion-Conducting Nanocomposite Polymer Blend Quasi-Solid Electrolytes for Dye-Sensitized Solar Cells

Vinoth Subramanian, Kamatam Hari Prasad, Himadri Tanaya Das, Kanimozhi Ganapathy, Satyanarayana Nallani,* and Thandavarayan Maiyalagan*



Cite This: *ACS Omega* 2022, 7, 1658–1670



Read Online

ACCESS |



Metrics & More

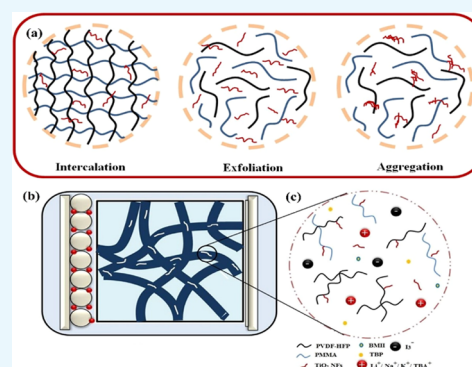


Article Recommendations



Supporting Information

ABSTRACT: Electrospun nanocomposite polymer blend poly(vinylidene difluoride-*co*-hexafluoropropylene) (PVDF-HFP)/poly(methyl methacrylate) (PMMA) membranes with a novel dispersion of x wt % of one-dimensional (1D) TiO₂ nanofiber fillers ($x = 0.0$ – 0.8 in steps of 0.2) were developed using the electrospinning technique. The developed nanocomposite polymer membranes were activated using various redox agents such as LiI, NaI, KI, and tetrabutyl ammonium iodide (TBAI). Introduction of the 1D TiO₂ nanofiber fillers improves the amorphous nature of the blended polymer membrane, as confirmed through X-ray diffraction (XRD) and Fourier transform infrared (FTIR), and yielded an electrolyte uptake of over 480% for a 6 wt % TiO₂ nanofiber filler-dispersed sample. PVDF-HFP/PMMA–1D 6 wt % TiO₂ nanofiber fillers with the LiI-based redox electrolyte provided a high conductivity of $2.80 \times 10^{-2} \text{ S cm}^{-1}$ and a power conversion efficiency (PCE) of 8.08% to their fabricated dye-sensitized solar cells (DSSCs). The observed better ionic conductivity and efficiency of the fabricated DSSCs could be due to the faster movement of the smaller-ionic-radius (Li) ions entrapped inside the amorphous polymer. This enhanced mobility of ions in the quasi-solid electrolyte leads to faster regeneration of the depleting electrons in the photoanode, resulting in improved efficiency. Further, the achieved high conductivity was analyzed in terms of the dynamics and relaxation mechanisms involved by the ionic charge carriers with complex impedance spectroscopy using a random barrier model and Havriliak–Negami formulation. It was observed that the high-conducting PVDF-HFP/PMMA–1D 6 wt % TiO₂ nanofiber fillers with LiI-based redox electrolyte show better ac conductivity parameters such as a σ of $5.82 \times 10^{-2} \text{ S cm}^{-1}$, ω_e (12685 rad s^{-1}), τ_e ($0.909 \times 10^{-4} \text{ s}$), and n (0.578). Also, dielectric studies revealed that the high-conducting sample has a higher dielectric constant and subsequently high loss. The J – V characteristics were studied using the equivalent circuit of a single-diode model, and the parameters influencing the photovoltaic performance were determined by Symbiotic Organisms Search (SOS) algorithm. The results suggest that the high-efficient sample possesses a minimum series resistance of 1.33 Ω and a maximum shunt resistance of 997 Ω . Hence, the highest-conducting electrospun-blended polymeric nanocomposite (PVDF-HFP–PMMA–6 wt % TiO₂ nanofiber fillers) with LiI-based redox agent and *tert*-butyl pyridine (TBP) additive as the polymer quasi-solid electrolyte nanofibrous membrane can be a better electrolyte for high-performance dye-sensitized solar cell applications.



1. INTRODUCTION

Photovoltaic technology is considered as the best method of producing energy, as it can convert photons to electrons without causing any environmental impact. Dye-sensitized solar cells (DSSCs) have been focused as a hopeful substitute towards the conventional solar cells as they are cost-effective and eco-friendly.¹ Recently, the highest power conversion efficiency (PCE) of 14% has been achieved for a cobalt(II/III) complex redox electrolyte solution.² The most crucial component of the DSSC is the electrolyte, which plays a significant function in the charge transport and dye regeneration. A high ion-conducting and chemically stable redox electrolyte is essential to improve the photovoltaic performance of DSSCs. Although higher efficiencies are

achieved by liquid electrolyte-based DSSCs, they suffer from serious problems such as leakage of the electrolyte due to low viscosity and poor sealing, evaporation at room temperature, deterioration of electrode materials, dissolution of the adsorbed sensitizer in the photoanode, short-circuiting, etc., which hinder their performance in the long run. A lot of effort

Received: July 10, 2021

Accepted: November 24, 2021

Published: January 3, 2022



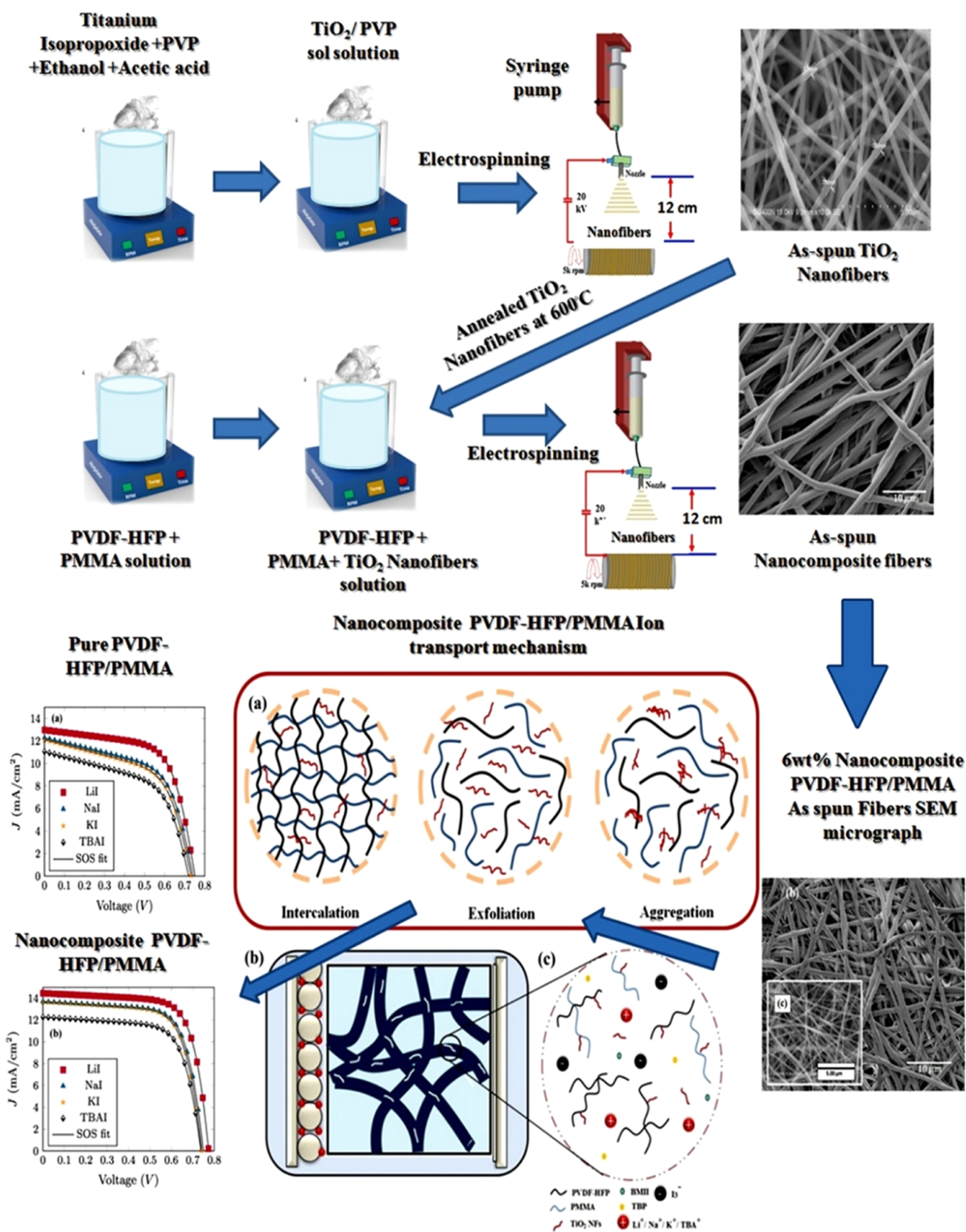


Figure 1. Schematic representation showing the preparation and ion transport mechanism. (a) Intercalation, exfoliation, and aggregation processes; (b) device architecture; (c) enlarged image of the different ions present inside the electrolyte of the developed novel nanocomposite electrospun-blended polymeric electrolyte membranes (PVDF-HFP–PMMA–6 wt % TiO₂ nanofiber fillers) with distinct iodide-based redox agents based on cations Li, Na, K, and TBA quasi-solid electrolyte.

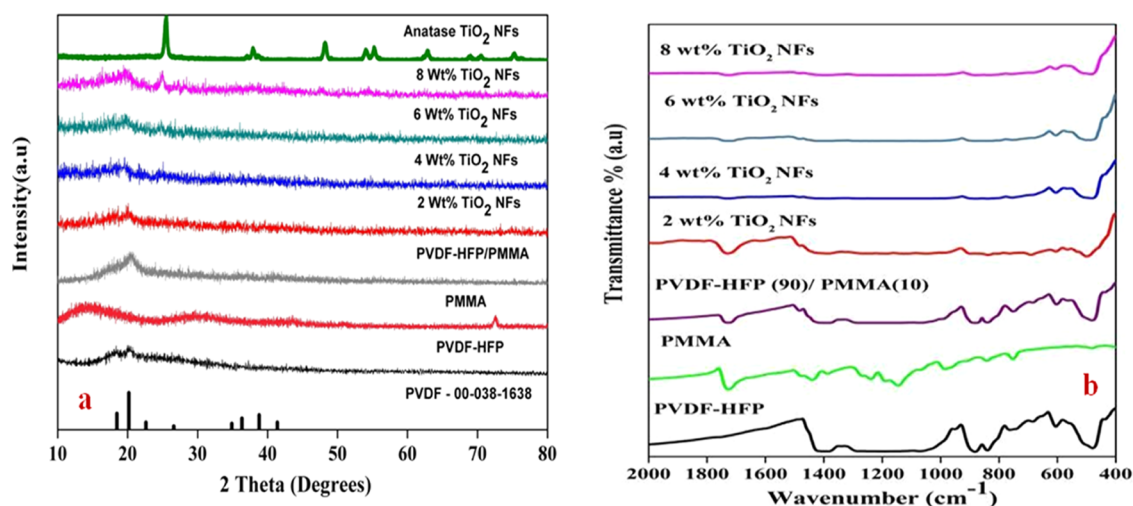


Figure 2. (a) XRD patterns, (b) Fourier transform infrared (FTIR) spectra of electrospun-blended polymeric membranes of PVDF-HFP–PMMA/*x* wt % of 1D TiO₂ nanofiber fillers.

has been taken to supersede liquid electrolytes by high-viscous gel electrolytes or polymer solid-state electrolytes, although they exhibit lower ionic conductivity.³ In polymer electrolytes, the spatial distribution of pores and their dimensions play a vital role in the intake of the electrolyte and the mobility of ions.^{3,4} However, the dimensions of the pores present in the electrolyte are influenced by the processing techniques, different one-dimensional (1D) and two-dimensional (2D) nanostructures, etc.⁵ Among several processing techniques, the electrospinning process has been successful in producing highly porous 1D nanofibrous polymer membranes that have a high surface area to entrap a huge quantity of fluid. Numerous polymers have been used as host matrices in the application of electrolytes for distinct applications such as lithium batteries, supercapacitors, DSSCs, electrocatalysts, etc.^{4–7} The host polymers include poly(vinylidene difluoride) (PVDF), poly(vinylidene difluoride-*co*-hexafluoropropylene) (PVDF-HFP), poly(acrylonitrile) (PAN), poly(methyl methacrylate) (PMMA), polystyrene (PS), poly(ethylene oxide) (PEO), etc., among which semicrystalline PVDF-HFP is utilized in many applications due to its favorable properties such as appreciable mechanical strength, highly stable electrochemical properties, and high dielectric constant ($\epsilon \approx 8.4$).^{8–15} PVDF-HFP is a copolymer in which PVDF is crystalline and HFP is amorphous, and the crystallinity is reduced by the HFP units in PVDF-HFP.¹⁶ Moreover, amorphous polymers exhibit ionic conductivity by the metamer motion of ions in the polymer strands. In order to raise the mobility of charge-carrying ions in the polymer matrix, various methods have been adopted in recent times, such as blending and co-polymerization, of which blending with a soft amorphous polymer is preferred. In this regard, various polymers such as PEO, PMMA, and their copolymers, including poly(ethylene carbonate-*co*-ethylene oxide) [P(EC-EO)], poly(vinylidene fluoride-trifluoro ethylene), and poly(methyl methacrylate-*co*-acrylonitrile-*co*-lithium methacrylate) (PMAML), are the most opted polymers that can be blended with PVDF-HFP.^{17,18} Among these, PMMA was selected for blending with PVDF-HFP in our present study, as it is highly amorphous in nature. Based on our conductivity results, a 9:1 proportion of the PVDF-HFP–PMMA sample is found to be more appropriate for electrolyte applications, as it has higher conductivity than other

compositions. Hence, the 9:1 composition of PVDF-HFP–PMMA is chosen for further optimization of crystallinity by the incorporation of inorganic fillers to form a nanocomposite polymer quasi-solid electrolyte.

Polymer matrix-based nanocomposites have become one of the interesting fields in recent times as they have numerous applications as electrolytes for dye-sensitized solar cells (DSSCs), lithium-ion batteries, supercapacitors, fuel cells, etc.^{19–21} Dispersal of nanosized inorganic ceramic fillers including Al₂O₃, ZnO, TiO₂, SiO₂, etc., into the polymer strands would help in their ready contact with the polar radicals present in the polymeric matrix by the chemical interaction of the Lewis acid–base and disrupt the crystallinity, resulting in the betterment of the intrinsic properties of the matrix, which favors conductivity.^{22–31} Addition of ceramic nanofillers into the polymeric matrix influences the rate of crystallization, degree of crystallinity, and melting enthalpy of the nanocomposite polymeric electrolyte.³² The reduction of crystallinity of the developed nanocomposite polymeric electrolyte membranes is caused by the crystallization in confined spaces. This results in a homogeneous and heterogeneous nucleation process with distinct pore size and pore volume. When a low content of nanofillers is incorporated, confined nucleation takes place to substitute the nanofillers in the primary nuclei to attain the spherule growth of crystallization, which leads to the intercalated nanocomposite formation.³³ At a higher concentration of nanofillers, the spherule growth is disrupted, which leads to confined crystallization in the nanopores of the polymer matrix.³⁴ The complete nanocomposite formation is achieved for an optimal concentration of nanofillers with exfoliation of the polymer strands. In the exfoliation process, the crystallinity would be drastically reduced, increasing the pathways for the transfer of ionic charges in the nanocomposite polymer electrolyte.^{35,36} Compared to the other inorganic ceramic fillers, TiO₂ nanofillers had better compatibility towards the TiO₂-based photoanode. Moreover, the higher dielectric constant of TiO₂ (≈ 86 – 170) can facilitate better dissociation with the polymer and hinder agglomeration in the polymer matrix. In this regard, novel TiO₂ nanofiber fillers are chosen to achieve exfoliated nanocomposite formation for the electrolyte in DSSC application. TiO₂ nanofibers embedded

in a blended electrospun polymeric matrix (PVDF-HFP–PMMA) might lead to a better mechanical durability and ion-conducting attributes on account of the dipolar nature and interaction of the Lewis acid–base radicals of TiO_2 with the polymer strands. To our knowledge, the dispersion of 1D nanofillers into the polymer host was not investigated until now. Electrospun 1D TiO_2 nanofibers dispersed in the blended polymer also exhibit a mesoporous morphology with a high surface area that can engulf more electrolytes, in addition to the nanofibrous structure of the polymer, and facilitate a 1D continuous channel for the transfer of ionic charges inside the polymer matrix. In the present study, distinct weight percentages of 1D TiO_2 nanofibers were dispersed in the PVDF-HFP–PMMA blend and electrospun to analyze its ion-conducting performance with distinct iodide–triiodide redox agents based on LiI/I_2 , NaI/I_2 , KI/I_2 , and tetrabutyl ammonium iodide (TBAI)/ I_2 . To understand the ion dynamics and relaxation mechanisms of the developed nanocomposite polymer quasi-solid electrolytes, the ion-conduction mechanism is analyzed using a random barrier model (RBM) and Havriliak–Negami (HN) formulation. The performance of the assembled DSSCs with the developed quasi-solid electrolytes is studied under 1 sun illumination (Figure 1).

2. RESULTS AND DISCUSSION

2.1. X-ray Diffraction (XRD) Analysis. Figure 2a depicts the XRD patterns of electrospun-blended polymeric nanocomposite membranes of PVDF-HFP–PMMA– TiO_2 with various contents (2, 4, 6, and 8 wt %) of 1D TiO_2 nanofibers as fillers. The XRD patterns of the electrospun-blended polymeric nanocomposite membranes of PVDF-HFP–PMMA– TiO_2 exhibit diffused and broad diffraction peaks at 18.2° (100) and 20.1° (020) compared with JCPDS data (38-1638), which confirms the formation of a semicrystalline nature of PVDF-HFP. The broadness of the diffraction peaks is due to the contents of TiO_2 . The observed peak-free XRD patterns of the PMMA confirm the amorphous phase. The intensity of the observed diffraction peak corresponding to PVDF-HFP drastically reduced for the blended polymeric sample due to blending with PMMA. This represents an enhancement in the amorphous character of the polymer blend PVDF-HFP–PMMA. The intensity of the XRD peaks still decreased with the incorporation of TiO_2 nanofibers up to 6 wt %. The diminishing intensity of the XRD peaks for the nanocomposite polymer blend samples is attributed to the intercalation of TiO_2 by the Lewis acid–base interaction between PVDF-HFP and TiO_2 .³⁷ The more amorphous nature of the electrospun-blended polymeric nanocomposite PVDF-HFP–PMMA– TiO_2 polymer blend would render many free pathways for conduction and increase the mobility μ of the charge carriers. Further increase in the contents of TiO_2 nanofiber fillers to 8 wt % leads to the emergence of the XRD peaks at 24 and 49° . These emergence of these XRD peaks is attributed to the crystallization of the anatase phase of TiO_2 nanofiber fillers inside the polymer matrix, which is compared with the JCPDS data (84-1285). The observed crystalline anatase phase of TiO_2 nanofiber fillers might be due to agglomeration of the TiO_2 nanofiber fillers, which may hinder the movement of ionic charges and in turn lower the conductivity of the nanocomposite PVDF-HFP–PMMA– TiO_2 sample for the 8 wt % content of TiO_2 nanofiber fillers.

2.2. FTIR Analysis. Figure 2b represents the FTIR spectra of pristine electrospun PVDF-HFP, PMMA, and PVDF-HFP–PMMA (9:1) blended polymeric thin-film membranes and nanocomposite PVDF-HFP–PMMA (9:1) with various contents (2, 4, 6, and 8 wt %) of 1D TiO_2 nanofiber fillers. The FTIR peaks noticed at 472 , 510 , 766 , 842 , 976 , 1279 , and 1408 cm^{-1} denote the distinctive characteristics of the PVDF-HFP ($-\text{CH}_2-\text{CF}_2-$) crystals.³⁸ The peaks at 766 , 531 , and 976 cm^{-1} are ascribed to the presence of the semicrystalline nature of α -PVDF-HFP. A prominent peak detected at the wavenumber 840 cm^{-1} reveals the proximity of β -PVDF-HFP to the rocking vibration modes of CH_2 . The wagging vibration modes of CF are observed at 472 cm^{-1} , which affirms the existence of pristine γ -PVDF-HFP. The peaks at the wavenumbers 510 and 1279 cm^{-1} are, respectively, due to the CF_2 bending vibrations and asymmetric stretching vibration modes.³⁹ The observed IR peaks corresponding to CH_2 rocking (752 cm^{-1}), CH_2 wagging (988 cm^{-1}), CH_2 scissoring (1485 cm^{-1}), and carbonyl $\text{C}=\text{O}$ (1733 cm^{-1}) correspond to the vibration modes of pristine PMMA. The distinctive peaks of 1159 , 1449 , and 1721 cm^{-1} are, respectively, assigned to $=\text{O}=\text{CH}_3$, CH_3 , and $\text{C}=\text{O}$ stretching vibration modes. The existence of the observed characteristic FTIR peaks of PVDF-HFP and PMMA ensures the good blending of the two polymers in the resultant membrane due to the intermolecular interaction between PVDF-HFP and PMMA. Furthermore, due to dispersion of various concentrations of nanocrystalline 1D TiO_2 nanofiber fillers (2, 4, 6, and 8 wt %) into the PVDF-HFP–PMMA blended polymeric matrix, a slight shift and a massive reduction in the transmission spectra of the FTIR peaks representing the crystalline phase of PVDF-HFP were observed, indicating the enhancement in the amorphous nature of the developed polymeric thin-film membranes. Moreover, upon the addition of the 1D TiO_2 nanofibers as fillers to the blended polymeric PVDF-HFP–PMMA, a wide band around the wavenumber range 600 – 450 cm^{-1} is detected, which is attributed to the stretching modes of vibration of crystalline anatase TiO_2 at 512 cm^{-1} .⁴⁰ Hence, the addition of PMMA and nanofillers has increased the amorphous property in the electrospun-blended polymeric nanocomposite PVDF-HFP–PMMA– TiO_2 membranes.

2.3. Scanning Electron Microscopy (SEM) Analysis. Figure 3a,b shows the surface morphologies of pristine blended polymeric electrospun PVDF-HFP–PMMA and electrospun-blended polymeric nanocomposite PVDF-HFP–PMMA/6 wt % 1D TiO_2 nanofibers as fillers, respectively. The inset of Figure 3b (i.e. Figure 3c) depicts the continuous nanofibrous morphology of crystalline anatase TiO_2 nanofibers calcined at 600°C with a mean fiber diameter of 250 nm. The SEM images exhibit a three-dimensional (3D) mesh-like morphology with the highly interconnected multifibrous stratum of continuously woven nanofibers. The interconnected stratum of the multifibrous network produces a mesoporous thin film that could imbibe and hold a greater quantity of electrolyte inside the membrane. The entrapping of more electrolytes in the membrane will increase the number of ionic charge carriers, and the porous nature of the membrane will also facilitate the transport of the ionic charge carriers, thereby improving the ionic conductivity. The mean fiber diameters of electrospun PVDF-HFP–PMMA pure and electrospun-blended polymeric nanocomposite PVDF-HFP–PMMA– TiO_2 nanofibers were found to be in the range of 300 – 350 nm . The variation in the AFD might be influenced by the variation in the concentration

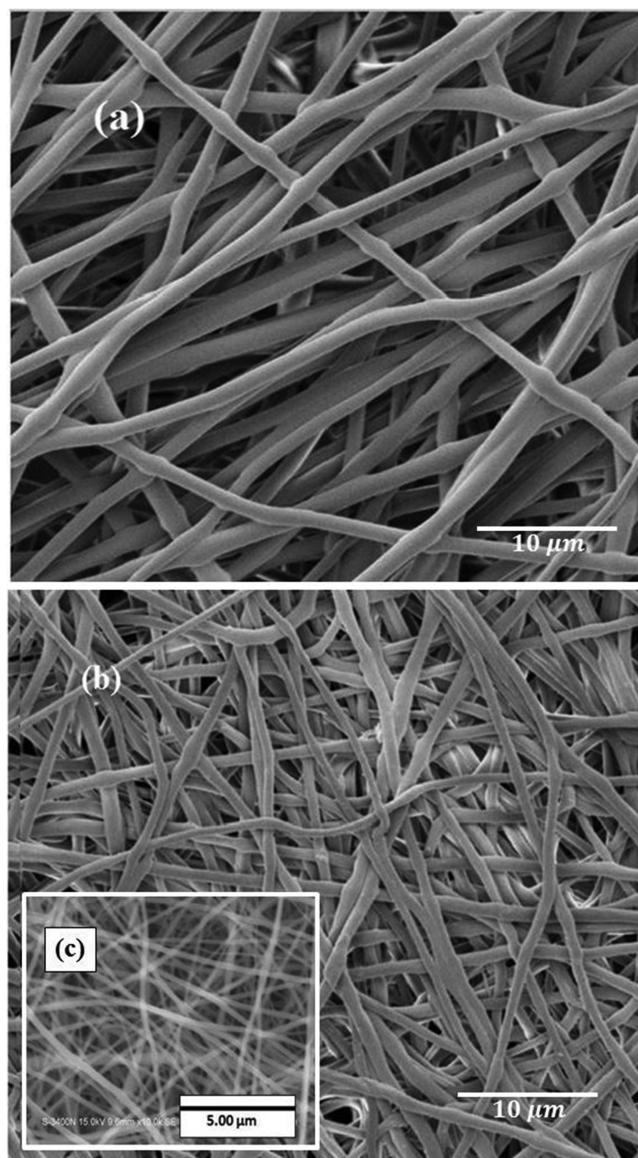


Figure 3. SEM micrographs. (a) Pure and electrospun-blended polymeric nanocomposite PVDF-HFP-PMMA. (b) Electrospun-blended polymeric nanocomposite membranes of PVDF-HFP-PMMA with 6 wt % of TiO_2 nanofiber fillers. (c) Electrospun crystalline anatase 1D TiO_2 nanofibers.

of the precursor solution upon addition of TiO_2 nanofibers despite keeping the electrospinning parameters constant for both the samples.

2.4. Electrolyte Uptake (EU) Analysis. All of the developed blended polymeric electrospun pristine and nanocomposite PVDF-HFP-PMMA- TiO_2 NF membranes were immersed in the developed ionic liquid electrolyte prepared using 0.5 M of ionic salts such as LiI, NaI, KI, and TBAI were individually added in 0.05 M I_2 , 0.6 M BMII, and 0.5 M of *tert*-butyl pyridine (TBP) were added in the mixture of a solvent consisting of ethylene carbonate (EC), propylene carbonate (PC), and acetonitrile (AN) (1:1:3, v/v/v). After imbibition of the electrolytes in each membrane, the excess electrolyte was removed by a tissue paper and the weights were determined individually. The electrolyte absorption capacity of all of the developed membranes was computed using eq 8. The calculated electrolyte uptake percentage was plotted against

the nanofiller concentration for various redox cation-based iodide-triiodide redox mediators as shown in Figure S1. Figure S1 reveals an enhanced electrolyte uptake percentage for various redox pairs up to 6 wt %. The highest electrolyte uptake percentage was noticed for the LiI-based electrolyte, which might pertain to the highly porous nature of the multifibrous morphology, as well as the coordination of TiO_2 with the polymer strands by Lewis acid-base interaction. Moreover, the crystalline TiO_2 nanofibers also possess a mesoporous nanofibrous structure that permeates a high quantity of the liquid electrolyte. Furthermore, the observed higher percent of electrolyte uptake for the Li-based redox electrolyte might be because of the smallest ionic radius of the cation lithium (Li) facilitating easy migration inside the polymer nanocomposite matrix among other cations used for the present study. On the other hand, PVDF-HFP-PMMA with 8 wt % of TiO_2 nanofiber fillers shows a reduction in uptake behavior, which might be associated with the agglomeration of the TiO_2 nanofiber fillers inside the polymer matrix, also confirmed by the XRD studies.

2.5. Impedance Studies. Figure 4a-d shows the room-temperature impedance spectra of electrospun-blended polymeric nanocomposite PVDF-HFP-PMMA/ x wt % of 1D TiO_2 nanofibers as fillers ($x = 0, 2, 4, 6,$ and 8) with various iodide-triiodide redox agents such as LiI/ I_2 , NaI/ I_2 , KI/ I_2 , and TBAI/ I_2 . In Figure 4, the impedance spectra of all of the developed blended polymeric nanocomposite PVDF-HFP-PMMA-based quasi-solid electrolyte membranes show a curved arc and a slanting spike. The arc observed at the high frequency denotes the bulk resistance, while the spike present at the low frequency elucidates the interfacial electrode-electrolyte double-layer capacitance effect as the constant-phase element (CPE). The x -intercept of the arc indicates the resistance (R_b). From Figure 4, it is inferred that the bulk resistances of the developed electrolyte membranes are lowered with the addition of nanofiller content equal to 6 wt % concentration and thereafter increase. The impedance spectra of the developed electrospun-blended polymeric nanocomposite (PVDF-HFP-PMMA- TiO_2 nanofibers with various redox electrolytes) quasi-solid electrolytes were fitted using the “WinFIT” software in accordance with its respective equivalent circuit. The conductivity of the developed electrolytes was computed using eq 9 and is presented in Table 1. The variation in the value of conductivity with respect to the nanofiller concentration is shown in Figure S1b, and the variation is similar to the electrolyte uptake behavior, as observed in Figure S1a.

The conductivity increased with the increase in concentration of the 1D nanofillers equivalent to 6 wt % and then reduced for 8 wt %. The reduction in conductivity might be ascribed to the aggregation of fillers that leads to an increase in crystallinity and can affect the porosity.⁴¹ The pristine and nanocomposite electrospun-blended polymeric membranes of PVDF-HFP-PMMA with 6 wt % of nanofibrous TiO_2 -activated in Li-based redox agent proved to have a high ionic conductivity of 0.253×10^{-2} and $2.80 \times 10^{-2} \text{ S cm}^{-1}$, respectively. From Table 1, it is found that 6 wt % of the 1D TiO_2 NF filler sample exhibits the highest value of conductivity among the developed electrolyte membrane samples with other nanofiller concentrations and distinct redox pairs. According to the values of conductivity of the developed electrolyte membranes, the better-conducting samples can be arranged in the order of iodide-triiodide redox agents as LiI/ I_2

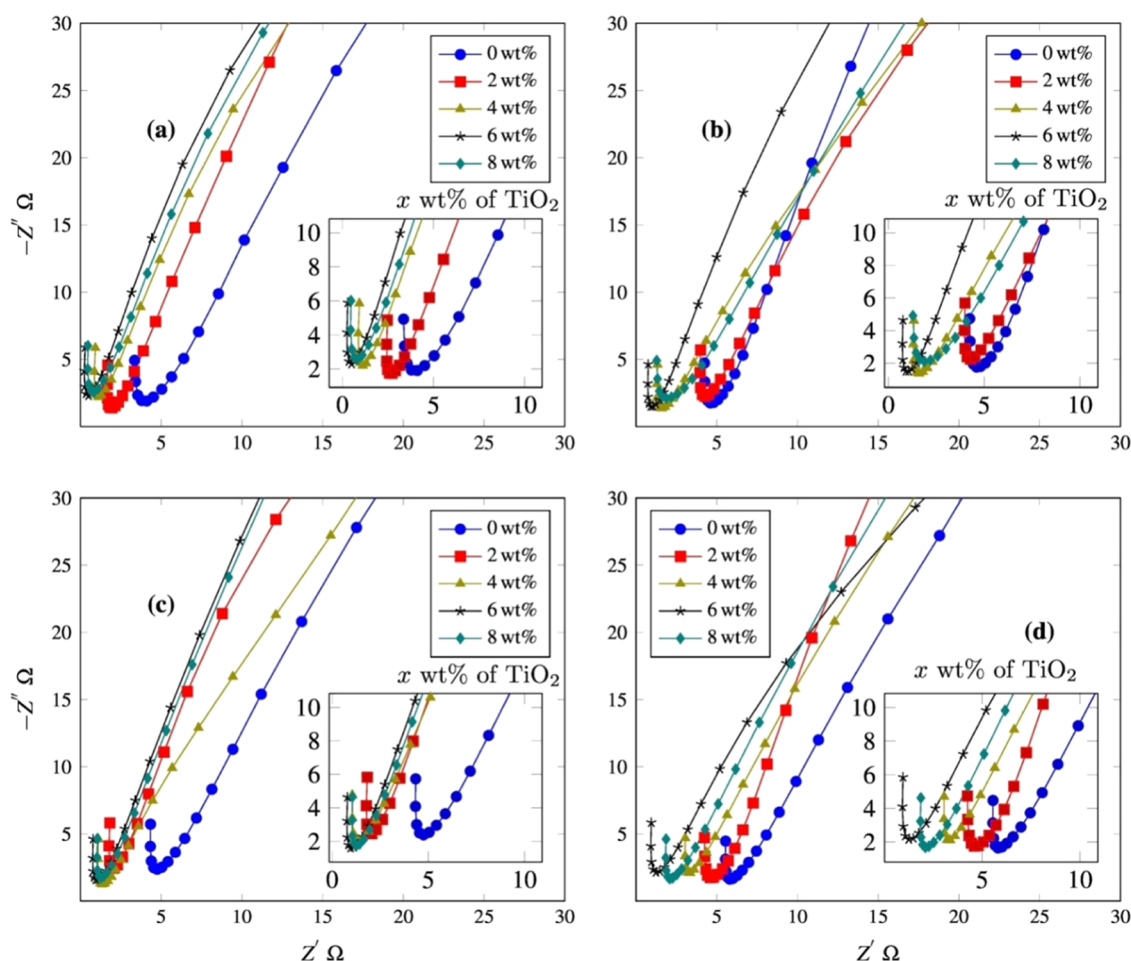


Figure 4. Nyquist plots of the developed PVDF-HFP-PMMA/ x wt % of TiO₂ NFs ($x = 0, 2, 4, 6,$ and 8) with distinct iodide-triiodide redox agents (a) LiI/I₂, (b) NaI/I₂, (c) KI/I₂, and (d) TBAI/I₂.

Table 1. Conductivity Values of Electrospun-Blended Polymeric Nanocomposite Membranes of PVDF-HFP-PMMA/ x wt % of TiO₂ NFs ($x = 0, 2, 4, 6,$ and 8) with Distinct Iodide-Triiodide Redox Agents LiI/I₂, NaI/I₂, KI/I₂, and TBAI/I₂

wt % of TiO ₂ NFs	σ (10^{-2} S cm ⁻¹)			
	LiI/I ₂	NaI/I ₂	KI/I ₂	TBAI/I ₂
0	0.253	0.215	0.181	0.174
2	0.729	0.693	0.328	0.298
4	1.24	1.03	0.829	0.425
6	2.80	1.50	1.36	1.09
8	1.59	1.09	0.787	0.645

> NaI/I₂ > KI/I₂ > TBAI/I₂. The observed variation may be ascribed to the size of the cations present in the redox species. Smaller cations might travel very easily within the polymeric matrix and can enhance the mobility of charge carriers, which in turn leads to high conductivity.⁴²

The ionic transport inside the electrolyte was analyzed in terms of the diffusion coefficient D , mobility μ , and number density n . The values of D , μ , and n of the developed electrospun-blended polymeric nanocomposite PVDF-HFP-PMMA-TiO₂ quasi-solid electrolyte membranes with Li-based redox electrolyte membranes were calculated using eqs 10, 13, and 14, respectively, and are shown in Table 2. In Table 2, the aggregate product values $n\mu$ of the number density and

Table 2. Ionic Transport Parameters (D , μ , and n) of Electrospun-Blended Polymeric Nanocomposite Membranes of PVDF-HFP-PMMA/ x wt % of TiO₂ NFs ($x = 0, 2, 4, 6$ and 8) with the Li-Based Redox Agent at Room Temperature (303 K)

wt % of TiO ₂	D (cm ²)	μ (cm ² V ⁻¹ s ⁻¹)	n (cm ⁻³)	$n\mu$
0	1.35×10^{-8}	5.15×10^{-7}	3.07×10^{22}	1.58×10^{16}
2	1.79×10^{-7}	6.84×10^{-6}	6.65×10^{21}	4.55×10^{16}
4	1.97×10^{-7}	7.53×10^{-6}	1.03×10^{22}	7.75×10^{16}
6	1.67×10^{-7}	6.38×10^{-6}	2.74×10^{22}	1.75×10^{17}
8	1.76×10^{-7}	6.73×10^{-6}	1.47×10^{22}	9.93×10^{16}

the mobility of the ionic carriers are shown incremented up to 6 wt %. The best electrolyte was distinguished with the highest value of the product $n\mu$. From Table 2, it is noticed that the developed electrospun-blended polymeric nanocomposite PVDF-HFP-PMMA-TiO₂ NF quasi-solid electrolyte sample with 6 wt % sample shows the highest value of 1.75×10^{17} as the product of $n\mu$.

2.6. AC Conductivity Studies. The frequency-dependent complex conductivity spectra (σ' and σ'') of PVDF-HFP-PMMA/ x wt % of TiO₂ NF membranes, developed by the electrospinning process and immersed in the respective iodide-triiodide redox agents, viz., LiI/I₂, NaI/I₂, KI/I₂, and TBAI/I₂, is given in Figure S2. The σ^* spectra with respect to

Table 3. Conductivity Parameters (σ , ω , τ_e , and n) Found by RBM Formulation for the Electrospun-Blended Polymeric Nanocomposite Membranes of PVDF-HFP-PMMA/ x wt % TiO₂ NFs ($x = 0, 2, 4, 6, 8$) with Distinct Iodide-Triiodide Redox Agents, viz., LiI/I₂, NaI/I₂, KI/I₂, and TBAI/I₂

wt % TiO ₂	σ (10^{-2} S cm ⁻¹)				ω_e (rad s ⁻¹)				τ_e (10^{-4} s)				n			
	Li	Na	K	TBA	Li	Na	K	TBA	Li	Na	K	TBA	Li	Na	K	TBA
0	2.83	0.375	0.475	0.517	4652	8433	7994	8098	2.15	1.19	1.25	1.23	0.329	0.294	0.235	0.194
2	5.31	0.698	0.507	0.542	7660	10 055	9658	8405	1.31	0.995	1.04	1.19	0.456	0.364	0.308	0.235
4	5.45	1.01	0.668	0.571	8837	10 276	10 055	9678	1.13	0.973	0.995	1.03	0.531	0.368	0.368	0.351
6	5.82	1.24	1.06	0.798	12 685	11 002	11 690	16 213	0.788	0.909	0.855	0.617	0.578	0.477	0.464	0.491
8	5.30	1.12	0.759	0.633	10 108	10 394	10 487	11 663	0.989	0.962	0.954	0.857	0.577	0.374	0.419	0.372

frequency show an enhancement in conductivity along with the increase in frequency, which is known as the polarization region, and then, the conductivity remains constant for a small frequency range, termed as the dc-conductivity region. In the high-frequency range, the conductivity keeps on increasing, which is due to dielectric dispersion. It is noted that the conductivity spectra curve rises with the increase in the weight percent of fillers up to an optimum concentration of 6 wt %, and then lowers for 8 wt % concentration. Moreover, the general three distinguishable regions are not observed, as the low-frequency and mid-frequency regions merge due to dominance in electrode polarization. The effect of electrode polarization has affected the edge of the onset of dc-conductivity. To understand the mechanism of ionic conduction and the crossover frequency at the onset of steady-state conduction, several hopping models have been discussed in the literature.^{43–47}

Among the models discussed, the random barrier model (RBM) describes the hopping of charge carriers over the randomly distributed energy barriers. The charge carriers hop over one barrier to the other and have a high probability to jump over the energy barrier with the lowest energy. RBM is considered to be the most realistic model to depict ion-conducting behavior mechanisms, as the charge carriers involved in the conduction process are assumed to be ions in this representation. In RBM formulation, the frequency-dependent conductivity σ^* is evinced as

$$\sigma^*(\omega) = \sigma_{dc} + \frac{i\omega\tau_e}{\ln(1 + i\omega\tau_e)} \quad (1)$$

where $\omega = 1/\tau_e$ is the frequency needed to overcome the biggest energy barrier, and σ_{dc} is the dc-conductivity at τ_e . The real σ' and imaginary σ'' parts of complex conductivity can be segregated as

$$\sigma'(\omega) = \frac{\sigma_{dc}\omega\tau_e \arctan(\omega\tau_e)}{\frac{\ln^2(1 + \omega^2\tau_e^2)}{4} + \arctan^2(\omega\tau_e)} \quad (2)$$

$$\sigma''(\omega) = \frac{\sigma_{dc}\omega\tau_e \ln^2(1 + \omega^2\tau_e^2)}{\frac{\ln^2(1 + \omega^2\tau_e^2)}{4} + \arctan^2(\omega\tau_e)} + \frac{A}{\omega^n} \quad (3)$$

The real σ' and imaginary σ'' parts of the experimentally measured data were fitted, respectively, to eqs 2 and 3 by Scipy's Levenburg–Marquardt method, and all of the obtained fitted parameters (σ_{dc} , ω , τ_e , and n) are shown in Table 3 for PVDF-HFP-PMMA/ x wt % of TiO₂ NF ($x = 0, 2, 4, 6, 8$ wt %) electrolyte membranes with iodide-triiodide redox agents based on cations Li, Na, K, and TBA.⁴⁸ The obtained values of

the parameters (σ_{dc} , ω , and n) increase with the addition of TiO₂ NF concentration equal to 6 wt % and then decrease.

The relaxation process of the charge carriers is described by the typical relaxation time (τ_e) required to overcome the randomly distributed energy barriers. The developed polymeric blended nanocomposite electrolytes show relaxation times ranging in the order of 10^{-4} s. Moreover, the value of τ_e reduces with the incorporation of TiO₂ NFs equal to 6 wt % concentration. The highly conducting, developed electrolyte sample depicts the characteristic frequency exponent (n) value of 0.578. The observed n value is found to be slightly >0.5 , which represents a change in the stochastic hopping to a one-dimensional orderly transport of ionic carriers inside the blended polymeric electrolyte sample.

In all of the plots, a similar behavior is perceived for conductivity. The σ_{dc} conductivity values of the developed blended polymeric nanocomposite PVDF-HFP-PMMA with TiO₂ NFs varies with respect to the iodide-triiodide redox agents based on cations in the order Li $>$ Na $>$ K $>$ TBA. This order of redox agents might be due to the bulky nature of cations in the electrolyte.

2.7. Dielectric Permittivity Studies. The dielectric constant ϵ' and dielectric loss ϵ'' of the developed electrolytes with respect to frequency are shown in Figure S3. It is observed that the high dielectric constant value ϵ' at lower frequencies is due to space charge polarization close to the interface between the electrode and electrolyte. The value of dielectric constant becomes almost constant at higher frequencies, represented as ϵ_∞ , which is ascribed to the instantaneous polarization of ions for an applied electric field with respect to the variation in time. The same kind of variation was noticed for dielectric loss ϵ'' . The experimental data of ϵ' and ϵ'' have been investigated by Havriliak–Negami (HN) formulation,^{49,50} in which the complex dielectric permittivity is given by

$$\epsilon^*(\omega) = \epsilon_\infty + \left[\frac{\epsilon_s - \epsilon_\infty}{[1 + (i\omega\tau_{HN})^{\alpha_{HN}}]^{\gamma_{HN}}} \right] \quad (4)$$

where ϵ_s and ϵ_∞ are, respectively, the static and high-frequency dielectric constants, τ_{HN} is the dielectric relaxation time, and α_{HN} and γ_{HN} are the asymmetric shape parameters with values $0 \leq \alpha_{HN} < 1$ and $0 \leq \alpha_{HN}\gamma_{HN} < 1$.

Table 4. Dielectric Parameters ($\Delta\epsilon$, α_{HN} , and β_{HN}) Evaluated by Havriliak–Negami Formulation for the Electrospun-Blended Polymeric Nanocomposite Membranes of PVDF-HFP–PMMA/ x wt % TiO₂ NFs ($x = 0, 2, 4, 6, \text{ and } 8$) with Distinct Iodide–Triiodide Redox Agents

wt % TiO ₂	$\Delta\epsilon$				α_{HN}				β_{HN}			
	LiI/I ₂	NaI/I ₂	KI/I ₂	TBAI/I ₂	LiI/I ₂	NaI/I ₂	KI/I ₂	TBAI/I ₂	LiI/I ₂	NaI/I ₂	KI/I ₂	TBAI/I ₂
0	34 378.27	25 111.90	33 555.21	36 053.15	0.0663	0.0783	0.3399	0.0632	3.0665	4.9437	0.0113	3.9076
2	487 040.4	39 195.99	37 592.56	36 415.98	0.5199	0.4618	0.3716	0.3402	1.1466	0.0338	0.8889	0.0146
4	348 274.9	55 669.31	37 616.72	33 794.82	0.6129	0.2493	0.3691	0.3228	2.076	0.2227	0.6596	0.0735
6	278 382.1	63 544.72	51 012.89	33 995.21	0.0259	0.3777	0.0423	0.1174	6.026	1.8162	1.313	2.911
8	441 511.4	60 850.73	40 871.54	30 649.54	0.0173	0.4067	0.0123	0.0181	2.156	1.7924	3.683	2.2086

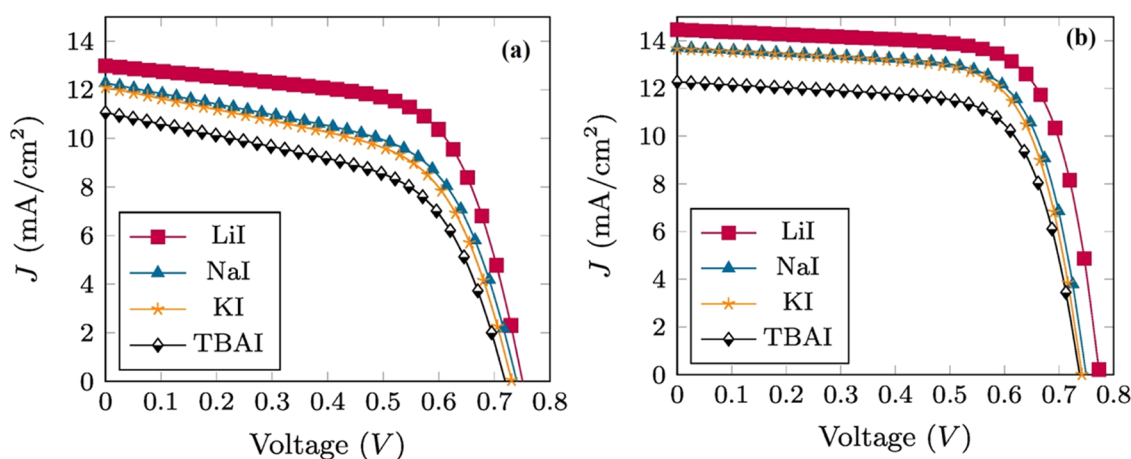


Figure 5. J – V operating characteristic curves of assembled DSSCs using pure blended polymeric nanocomposite (a) PVDF-HFP–PMMA and (b) PVDF-HFP–PMMA–6 wt % TiO₂ NF electrolyte membranes with distinct redox along with the Symbiotic Organisms Search (SOS) fit.

$$\epsilon'(\omega) = \epsilon_{\infty} + (\epsilon_s - \epsilon_{\infty}) \left[1 + 2(\omega\tau_{\text{HN}})^{\alpha_{\text{HN}}} \cos\left(\frac{\alpha_{\text{HN}}\pi}{2}\right) + (\omega\tau_{\text{HN}})^{2\alpha_{\text{HN}}} \right]^{-\alpha_{\text{HN}}/2} \cos \left[\arctan \left(\frac{\sin\left(\frac{\alpha_{\text{HN}}\pi}{2}\right)}{(\omega\tau_{\text{HN}})^{-\alpha_{\text{HN}}} + \cos\left(\frac{\beta_{\text{HN}}\pi}{2}\right)} \right) \right] \quad (5)$$

The imaginary part is expressed as

$$\epsilon''(\omega) = (\epsilon_s - \epsilon_{\infty}) \left[1 + 2(\omega\tau_{\text{HN}})^{\alpha_{\text{HN}}} \cos\left(\frac{\alpha_{\text{HN}}\pi}{2}\right) + (\omega\tau_{\text{HN}})^{2\alpha_{\text{HN}}} \right]^{-\alpha_{\text{HN}}/2} \sin \left[\arctan \left(\frac{\sin\left(\frac{\alpha_{\text{HN}}\pi}{2}\right)}{(\omega\tau_{\text{HN}})^{-\alpha_{\text{HN}}} + \cos\left(\frac{\beta_{\text{HN}}\pi}{2}\right)} \right) \right] + \frac{S}{\omega^n} \quad (6)$$

The term S/ω^n in eq 6 explains the existence of interfacial polarization. Figure S3 presents the frequency-dependent real and imaginary dielectric spectra of the electrospun-blended polymeric nanocomposite electrolytes PVDF-HFP–PMMA/ x wt % of TiO₂ NFs ($x = 0, 2, 4, 6, 8$) with the respective distinct iodide–triiodide redox agents based on cations Li, Na, K, and TBA. From Figure S3, it is observed that the value of dielectric constant ϵ' gradually decreases as the frequency of the input signal increases, and then a constant ϵ' is observed at the high-frequency range. The variation in the ϵ' at low-frequency range is attributed to the effect of electrode polarization. The dielectric constant of the developed samples shows enhance-

ment with the addition of TiO₂ NFs equal to 6 wt % concentration, implying that it exhibits high conductivity among the developed compositions. The developed high-conducting electrolyte sample possesses a high dielectric constant and subsequently high loss. In order to analyze the non-Debye relaxation behavior of the developed electrolyte samples, Havriliak–Negami (HN) formulation is used. The ϵ' and ϵ'' data were fitted using eqs 14 and 15, by applying Scipy's Levenberg–Marquardt method. The obtained fitted dielectric parameters of the developed electrospun-blended polymeric nanocomposite PVDF-HFP–PMMA–TiO₂ NFs with iodide–triiodide redox agents based on cations Li, Na, K, and TBA are shown in Table 4. In Table 4, an enhanced dielectric strength $\Delta\epsilon$ can be observed for 6 wt % composition of the electrolyte. The observed two asymmetric shape parameters (α_{HN} , β_{HN}) reveal the non-Debye relaxation behavior of ionic conductivity. Among all combinations of the developed electrolytes with the respective redox agents, 6 wt % composition shows the highest δ , which implies high polarizability.

The dielectric strength of the developed electrospun-blended polymeric nanocomposite electrolytes PVDF-HFP–PMMA with TiO₂ NFs varies in accordance with the presence of the iodide–triiodide redox agents based on cations in the order Li > Na > K > TBA. Obviously, Li-based PVDF-HFP–PMMA with 6 wt % TiO₂ NF electrolyte shows the highest δ . The observed inference very well supports the complex conductivity analysis.

2.8. Performance of the Fabricated DSSCs. Figure 5a,b displays the J – V curves of the DSSCs fabricated with electrospun-blended polymeric pure PVDF-HFP–PMMA (0 wt %) and electrospun-blended polymeric nanocomposite electrolyte fibrous membranes PVDF-HFP–PMMA–6 wt %

Table 5. Photovoltaic Parameters of the DSSCs Fabricated Using Pure Blended Polymeric Electrolyte (PVDF-HFP-PMMA-0 wt % 1D TiO₂) and Blended Polymeric Nanocomposite (PVDF-HFP-PMMA-6 wt % 1D TiO₂) Electrolyte Membranes with Distinct Redox Pairs

redox couple	V _{oc} (V)		J _{sc} (mA cm ⁻²)		J _o (nA cm ⁻²)		R _s (Ω)		R _{sh} (Ω)		n		FF		(η%)	
	0 wt %	6 wt %	0 wt %	6 wt %	0 wt %	6 wt %	0 wt %	6 wt %	0 wt %	6 wt %	0 wt %	6 wt %	0 wt %	6 wt %	0 wt %	6 wt %
LiI	0.756	0.773	13.12	14.48	1.67	1.66	4.54	1.33	439	997	1.846	1.88	63.556	72.268	6.304	8.089
NaI	0.742	0.751	12.57	13.74	1.68	1.66	5.36	2.17	226	874	1.845	1.828	56.052	70.619	5.228	7.287
KI	0.731	0.742	12.41	13.69	1.66	1.66	5.54	2.34	214	841	1.825	1.81	55.083	70.112	4.997	7.122
TBAI	0.72	0.738	11.36	12.31	1.66	1.66	5.62	2.49	209	819	1.81	1.813	53.807	69.820	4.401	6.343

TiO₂ nanofibers, respectively, activated in distinct redox electrolyte solutions serving as electrolytes and pretreated TiCl₄ and TiO₂ nanofibers (P25) serving as photoanodes. The photovoltaic performance data such as open circuit voltage (V_{oc}) and short-circuit current density (J_{sc}) were obtained from the *J*-*V* curves, whereas fill factor (FF) and power conversion efficiency (PCE) (η%) were calculated using eqs 15 and 16. The obtained photovoltaic parameters are tabulated in Table 5. It was inferred that the DSSCs fabricated with the Li-based redox agent reveals a higher PCE of 8.089% among all DSSCs assembled with Na-, K-, TBA-based redox agents. Moreover, the J_{sc} value for the DSSC with the Li-based redox agent was noted to have the highest value of 14.48 mA cm⁻², which can be attributed to the higher ionic conductivity of the electrolyte that proceeds with fast regeneration in the redox ingredients and is successively followed by uninterrupted regeneration of the dye. The continuous regeneration of the dye and redox components restricts the negative effect of recombination during the operation of the DSSCs. Furthermore, the pretreated fluorine-doped tin oxide (FTO) acts as a blocking layer for the photoanode and controls recombination, which might also enhance the J_{sc}. Although V_{oc} seems to be constant, some variations are noticed, which might be due to the influence of the cations existing in the redox mediator. The cations present in the electrolyte would alter the Fermi energy level of the photoanode. The performance of the DSSCs was in accordance with the size of the cations present in the electrolyte. Simultaneous electrochemical impedance spectroscopy (EIS) measurement of the fabricated DSSCs is time consuming, and maintaining a steady state of the DSSCs during the experiment is difficult. The temperature of the DSSCs varies due to incident radiation for a longer period.⁵¹ Furthermore, the analysis of EIS data requires a complex process of fitting to a suitable equivalent circuit of the impedance model and interpreting the parameters. Therefore, a simple and faster method is required to determine the parameters. The *J*-*V* characteristic data of the fabricated DSSCs were analyzed by the single-diode model of the photovoltaic cell. The intrinsic parameters (J_{sc}, J_o, R_s, R_{sh}, and *n*) that influence the photovoltaic performance of the cell were estimated by incorporating a meta-heuristic Symbiotic Organisms Search (SOS) algorithm in an IPython platform.^{52,53} The photocurrent density (*J*) can be explicitly represented according to the single-diode model as

$$J = J_{sc} - J_o \left[\exp \left(\frac{q(V + R_s J)}{nkT} \right) - 1 \right] - \frac{V + J R_s}{R_{sh}} \quad (7)$$

where J_{sc} denotes the short-circuit current density, J_o represents the dark photocurrent density, *V* is the applied voltage, R_s is the series resistance, R_{sh} is the shunt resistance, *n* is the diode ideality factor, *k* is the Maxwell Boltzmann constant, and *T* is

the operating temperature of the device. The internal parameters of the fabricated DSSCs were obtained by minimizing the root-mean-square error (RMSE) between the experimental *J*-*V* characteristic data and the simulated *JV* characteristic data evaluated from the single-diode model equation through the SOS algorithm applied in IPython platform. The intrinsic parameters responsible for the performance of the device were obtained by the best fit of the experimental and simulated *J*-*V* curves with a minimum value of RMSE. The obtained internal parameters of the fabricated DSSCs are shown in Table 5.

From Table 5, it is observed that the value of R_s has decreased for the fabricated DSSCs with the addition of 6 wt % TiO₂ NFs, whereas the value of R_{sh} has increased for the fabricated DSSCs' nanocomposite electrolyte. The low value of R_s prohibits the negative recombination reactions with the dye and the electrolyte, and facilitates faster transport of charge carriers in the photoanode material. The high value of R_{sh} accelerates the regeneration process involved by the redox agents and the dye. In Table 5, the DSSCs fabricated with LiI-based electrolytes show a lower value of R_s and higher value of R_{sh} compared with other redox agents (Na, K, and TBA), which favors a better photovoltaic performance of the device. By the incorporation of one-dimensional nanofibrous TiO₂, the values of R_s and R_{sh} were further improved, due to the increase in amorphous nature of the blended polymeric matrix.

From the conductivity studies, the electrospun PVDF-HFP-PMMA/6 wt % TiO₂ nanofiber fillers with various redox agents were noticed to be high-conducting electrolytes. R_s is anticipated to have a low value and R_{sh} should have a high value for enhanced FF and η% of the cell. From Table 5, it is noticed that the DSSCs fabricated with Li-based electrospun-blended polymeric nanocomposite PVDF-HFP-PMMA-6 wt % of 1D TiO₂ reveal a low value of R_s and a high value of R_{sh} in comparison with the DSSCs fabricated by other redox agents, which might be due to the smaller cationic radius of lithium.

3. CONCLUSIONS

Fast ion-conducting nanocomposite (PVDF-HFP-PMMA-TiO₂ nanofiber fillers) polymer quasi-solid electrolyte nanofibrous membranes were developed with various iodide-triiodide redox agents based on cations Li, Na, K, and TBA as electrolyte solutions using the electrospinning method as well as electrolyte uptake (EU) measurement. All of the developed nanocomposite polymer quasi-solid electrolyte nanofibrous membranes were characterized using XRD, FTIR, differential scanning calorimetry (DSC), and SEM. The conductivity of all of the developed nanocomposite polymer quasi-solid electrolyte samples was evaluated by analyzing the measured impedance data using WinFIT software. It is found that the PVDF-HFP-PMMA-1D 6 wt % TiO₂ with Li-based redox

nanocomposite polymer quasi-solid electrolyte exhibits the highest conductivity of $2.80 \times 10^{-2} \text{ S cm}^{-1}$. The evaluated conductivity and dielectric permittivity data were, respectively, analyzed using a random barrier model and Havriliak–Negami formulation, and it was found that the developed electrospun-blended polymeric nanocomposite polymer blend quasi-solid electrolyte nanofibrous membranes exhibit the non-Debye behavior of conduction mechanism.

Dye-sensitized solar cells (DSSCs) were fabricated using the developed electrospun-blended polymeric nanocomposite polymer blend quasi-solid electrolyte nanofibrous membranes, and it was found that PVDF-HFP-PMMA-6 wt % TiO_2 nanofiber fillers with Li-based redox agent and TBP additive achieved the highest power conversion efficiency (η) of 8.09%. The power conversion efficiency (PCE) ($\eta\%$) was evaluated for all of the developed DSSCs using the measured voltage and current density data. It is found that the DSSCs fabricated using electrospun-blended polymeric nanocomposite polymer blend quasi-solid electrolyte nanofibrous membrane exhibits the highest power conversion efficiency (PCE) of 8.08%. Hence, the highest-conducting electrospun-blended polymeric nanocomposite (PVDF-HFP-PMMA-6 wt % TiO_2 nanofiber fillers) with Li-based redox agent and TBP additive as the polymer quasi-solid electrolyte nanofibrous membrane can be a promising electrolyte for high-performance dye-sensitized solar cell applications. The J - V characteristic data of the fabricated DSSCs were analyzed by an equivalent circuit of the single-diode model and the intrinsic parameters influencing the photovoltaic performance were determined by the SOS algorithm.

4. EXPERIMENTAL SECTION

4.1. Materials. Poly(vinylidene difluoride-*co*-hexafluoropropylene) ($M_w = 500\,000$), poly(methyl methacrylate) ($M_w = 300\,000$), titanium isopropoxide (97%), *tert*-butyl pyridine (TBP), ethylene carbonate (EC), and propylene carbonate (PC) were procured from Sigma-Aldrich. Poly(vinylpyrrolidone) (PVP, $M_w = 1\,300\,000$) and iodide-based compounds such as iodine (I_2), *n*-butyl-3-methyl imidazolium iodide (BMII), potassium iodide (KI), lithium iodide (LiI), sodium iodide (NaI), and tetrabutyl ammonium iodide (TBAI) were purchased from Alfa Aesar. Solvents such as acetone, acetonitrile (AN), and *N,N*-dimethyl acetamide (DMAc) were procured from Merck. 1D TiO_2 nanofiber fillers were synthesized by electrospinning methods. All of the utilized chemicals are analytical grade and were used without any further purification procedures.

4.2. Synthesis of TiO_2 Nanofibers. One milliliter of titanium isopropoxide was dissolved in a mixture of solvents containing acetic acid and ethanol in the ratio (2:2) under constant stirring using a magnetic stirrer to obtain a homogeneous sol solution. Then, a polymer solution was developed by dissolving 0.53 g of PVP in 6 mL of ethanol under constant stirring. The sol solution and the polymer solution were mixed gradually under constant magnetic stirring until a homogeneous solution with adequate viscosity was obtained. The resultant homogeneous composite polymeric (PVP/ TiO_2) viscous solution was filled in a new sterile syringe with a stainless-steel needle size of 21 gauge and with 0.71 mm as the diameter for the process of electrospinning. The length of the space between the syringe's needle tip to the grounded rotating drum was fixed at 12 cm, and the solution was injected with the flow rate fixed at the pump as 1.5 mL h^{-1} . The

rotating drum, made of stainless steel (SS), was covered with a piece of foil made of aluminum. A very high electric potential of 18 kV was supplied within the metallic needle, and the formed electrospun composite (TiO_2 /PVP) nanofibers were collected around an aluminum foil. The resultant composite (TiO_2 /PVP) nanofibers were calcined at $600 \text{ }^\circ\text{C}$ at $20 \text{ }^\circ\text{C min}^{-1}$ rate of heating for 3 h to get the crystalline anatase TiO_2 nanofibers.

4.3. Synthesis of Nanocomposite Polymer Blend Nanofibrous Membranes. The polymeric blend solution was prepared by taking 16 wt % of 9:1 (w/w) ratio of two polymers such as PVDF-HFP and PMMA, dissolved in a solvent mixture comprising DMAc and acetone (3:7, v/v). The obtained solution was stirred vigorously for 3 h at room temperature under magnetic stirring to obtain a homogeneous polymer blend solution. Subsequently, different (2, 4, 6, and 8 wt %) concentrations of 1D TiO_2 nanofibers, already synthesized by the electrospinning technique, were added slowly to the obtained precursor solution under steady magnetic stirring to form a whitish viscous optimal solution. The whitish precursor blended polymeric nanocomposite solution was filled in a 10 mL syringe with a metallic needle of thickness 24 gauge. The solution-filled syringe was loaded in an electrospinning instrument by fixing the distance between the rotating drum collector and the tip of the needle as 12 cm. In the electrospinning instrument, the feed rate of the solution was adjusted to 1.25 mL h^{-1} . The speed of rotation of the rotating drum was adjusted to 500 rpm. A constant high voltage of about 18 kV was subjected between the drum and the metallic needle. The electrospun nanofibers were gathered over an aluminum foil wrapped around the rotating drum. The electrospun nanofibrous blended polymeric film was peeled out from the wrapped aluminum foil and dehydrated at $60 \text{ }^\circ\text{C}$ for 24 h to remove the remnant solvents. The mean thickness of the developed thin-film membranes was observed to be in the range of 60–100 μm , which was measured using a digital meter.

4.4. Characterization. Various characterization techniques were followed to evaluate the structural, morphological, electrolyte uptake, and electrochemical properties of the prepared samples, and finally, the photovoltaic performance of the fabricated DSSCs was analyzed. The structural characterization of the nanocomposite membranes dispersed with distinct concentrations of TiO_2 nanofibers was studied using an XRD (PANalytical X-pert PRO (Philips) diffractometer) comprising a copper target that emitted $\text{Cu K}\alpha$ radiation with a wavelength of $\lambda = 1.54060 \text{ \AA}$. The XRD patterns were recorded between 10 and 80° with a step size of 1.27° , which was functioned at 30 mA and 40 kV. The surface morphology of the developed nanocomposite membranes were analyzed by SEM micrograph images (SEM, Zeiss). FTIR spectra were recorded by a Nicolet 6700 spectrophotometer in the spectral range of $2000\text{--}400 \text{ cm}^{-1}$ with a high resolution of about 4 cm^{-1} .

The electrolyte uptake capacities of all of the developed electrospun-blended polymeric nanocomposite fibrous membranes were determined by immersing them in an electrolyte solution containing iodide–triiodide redox agents such as LiI/I_2 , NaI/I_2 , KI/I_2 , and TBAI/I_2 separately for 2 h. After immersing, the activated electrolyte membranes were pressed mildly using a tissue paper to extract the excess content of liquid electrolyte used in the electrolyte uptake process and then weighed.

The percent of electrolyte uptake (EU %) was evaluated using

$$\text{EU\%} = \frac{W_1 - W_0}{W_0} \times 100 \quad (8)$$

where W_0 and W_1 are, respectively, the weight of dry and wet membranes. The developed electrospun-blended polymeric nanocomposite fibrous membranes embedded with various concentrations of TiO_2 nanofiber fillers ($x = 2, 4, 6, 8$ wt %) immersed in electrolyte solutions containing iodide–triiodide redox agents such as LiI/I_2 , NaI/I_2 , KI/I_2 , and TBAI/I_2 were sandwiched in between two electrodes made up of stainless steel (SS). The SS electrodes are known as blocking electrodes, and the impedance data were measured by a high-frequency response analyzer (Novocontrol, Montabaur, Germany) within the range of frequency 1 mHz to 1 MHz. The ionic conductivity of electrospun-blended polymeric nanocomposite quasi-solid electrolyte solutions containing iodide–triiodide redox agents was computed by the following mathematical expression

$$\sigma = \frac{t}{R_b A} \text{ S cm}^{-1} \quad (9)$$

where σ represents the conductivity, t denotes the thickness of the developed polymeric electrolyte membrane (in cm), A refers to the area (in cm^2) of the membrane, and R_b denotes the bulk resistance (in Ω) of the developed electrolyte membranes.

In order to study the ionic transport of the developed nanocomposite quasi-solid electrolytes, the diffusion coefficient (D), the mobility of ions (μ), and the number density (n) are calculated at room temperature (303 K) using the following equations.

The diffusion coefficient of the ions is expressed as

$$D^2 = \frac{d^2}{\tau \delta^2} \quad (10)$$

where $\tau = 1/\omega$, τ is the relaxation time, ω is the angular frequency at which the inclined spike cut the x -axis of the Nyquist plots, $\delta = d/\lambda$, $d = t/2$, t is the thickness of the developed membrane, and λ is the thickness of the electrical double layer, expressed as

$$\lambda = \frac{\epsilon' \epsilon_0 A}{k^{-1}} \quad (11)$$

where A is the area of the developed membrane, k^{-1} is the capacitance of a constant-phase element obtained by fitting the Nyquist plots, and ϵ_0 is the permittivity of free space. The dielectric constant can be evaluated using the following expression

$$\epsilon' = \left(\frac{t}{\omega \epsilon_0 A} \right) \frac{Z''}{Z'^2 + Z''^2} \quad (12)$$

The mobility of the ions is given by

$$\mu = \frac{eD}{k_B T} \quad (13)$$

where k_B is the Maxwell–Boltzmann constant and e is the electric charge (1.6×10^{-19} C). The number density is expressed as

$$n = \frac{\sigma}{e\mu} \quad (14)$$

where σ is the conductivity of the sample.

The photovoltaic performance of the DSSCs was measured using a solar simulator (Photo Emission Tech, Inc. (PET)), with the spectral power measured by a standard AM 1.5G filter. The photocurrent density–voltage (J – V) curves were simultaneously recorded by an electrochemical system (BIO-LOGIC SP-50, France) with an input power of 100 mW cm^{-2} . The photovoltaic performance of the developed quasi-solid polymer electrolyte with 1D TiO_2 nanofibers was studied in terms of fill factor (FF) and power conversion efficiency (PCE %). The fill factor is calculated using the expression

$$\text{FF} = \frac{V_m I_m}{V_{oc} J_{sc}} \quad (15)$$

where V_m and I_m are, respectively, the maximum value of voltage and current

$$\text{PCE} (\eta\%) = \frac{V_m I_m}{P_{in}} \times 100 \quad (16)$$

where P_{in} is the incident power.

4.4.1. Fabrication of DSSCs. The fabrication of DSSCs involves the preparation of distinct components such as a sensitized photoanode (TiO_2), a platinized counter electrode, and a quasi-solid electrolyte. The fluorine-doped tin oxide (FTO, $\text{SnO}_2\text{:F}$ $7 \Omega \text{ sq}^{-1}$, purchased from Solaronix TEC7) glass slides act as a transparent conducting oxide (TCO) for the anode and cathode layers of the DSSCs. The FTO glasses were washed with de-ionized water and ethanol and then dried. To introduce a blocking layer for retarding the recombination effect, the FTO glasses were drenched in 40 mM solution of TiCl_4 , prepared by dissolving the fumes of TiCl_4 in distilled water at $70 \text{ }^\circ\text{C}$ for 30 min. After the pretreatment with TiCl_4 , the FTO slides were washed with distilled water and ethanol. In all, 0.4 g of TiO_2 (P25 with the nanoparticle size ranging from 25 to 30 nm), acetic acid, Triton-X, and ethanol were mixed and ground using a mortar for half an hour to form a colloidal paste of TiO_2 .

The colloidal suspension of TiO_2 paste was spread over an area of 0.25 cm^2 as a thin film with a thickness of $15 \mu\text{m}$ on the FTO glass by the doctor blade technique. The TiO_2 -coated plates were sintered at $450 \text{ }^\circ\text{C}$ in order to remove the organic solvents and surfactant used in the preparation of the suspension, and then gradually cooled at $80 \text{ }^\circ\text{C}$. Then, the plates were immersed in the dye solution of 0.5 mM ruthenium red dye (N719 purchased from Sigma-Aldrich), mixed in a mixture of solvents containing ethanol and acetonitrile in the ratio 2:1 for 24 h, and kept in a dark room to prohibit the absorption of light while sensitizing. After sensitizing, the developed photoanodes were rinsed in isopropanol to remove the extra dye and then dried out at room temperature. Simultaneously, the counter electrodes were developed by coating hydrogen hexachloro platinic acid mixed in acetonitrile solution as a thin film by the drop casting technique onto the active area of the FTO glass plates and sintered at $450 \text{ }^\circ\text{C}$. In order to introduce a spacer layer on the photoanode to prevent short-circuiting, a Surlyn tape of thickness 19 mm was pasted around the active area.

The quasi-solid electrolyte with 1D TiO_2 nanofillers was developed by dipping the developed electrospun-blended polymeric nanocomposite membranes in the liquid electrolyte

containing 0.5 M redox cationic salts (LiI, NaI, KI, TBAI) individually; 0.05 M I₂, 0.6 M BMII, and 0.5 M *tert*-butyl pyridine were mixed in a solvent mixture of acetonitrile/EC/PC (3:1:1, v/v/v). The excess liquid electrolyte was wiped away with a tissue paper; all of the developed quasi-solid electrolytes were then sandwiched between the dye-sensitized TiO₂ photoanode and the platinized counter electrode and bound by clips. Figure 1 shows the schematic representation of the preparation of the polymer electrolyte samples, and the ion transport mechanism due to intercalation, exfoliation, and aggregation processes with the incorporation of fillers. Also, the figure shows the performance of the DSSCs fabricated with the nanocomposite quasi-solid electrolytes.

■ ASSOCIATED CONTENT

SI Supporting Information

The Supporting Information is available free of charge at <https://pubs.acs.org/doi/10.1021/acsomega.1c03644>.

Electrolyte uptake and variation of conductivity of composites (Figure S1); the conductivity spectra of polymeric composites (Figure S2); the dielectric spectra of electrospun-blended polymeric nanocomposite membranes of PVDF-HFP-PMMA/*x* wt % of TiO₂ NFs (*x* = 0, 2, 4, 6, 8) with distinct iodide-triiodide redox agents (a) LiI/I₂ (b) NaI/I₂ (c) KI/I₂ and (d) TBAI/I₂ (Figure S3) (PDF)

■ AUTHOR INFORMATION

Corresponding Authors

Satyanarayana Nallani – Department of Physics, Pondicherry University, Puducherry 605014, India; orcid.org/0000-0003-0499-6346; Email: nallanis2011@gmail.com

Thandavarayan Maiyalagan – Department of Chemistry, SRM institute of Science and Technology, Kattankulathur, Tamil Nadu 603203, India; orcid.org/0000-0003-3528-3824; Email: maiyalagan@gmail.com

Authors

Vinoth Subramanian – Department of ECE, Manakula Vinayagar Institute of Technology, Puducherry 605014, India

Kamatam Hari Prasad – Department of Physics, Institute of Aeronautical Engineering, Hyderabad 500043, India

Himadri Tanaya Das – Centre of Advanced Materials and Applications, Utkal University, Bhubaneswar, Odisha 751004, India

Kanimozhi Ganapathy – Department of Physics, Pondicherry University, Puducherry 605014, India

Complete contact information is available at:

<https://pubs.acs.org/10.1021/acsomega.1c03644>

Notes

The authors declare no competing financial interest.

■ ACKNOWLEDGMENTS

S.N. acknowledges the UGC, Govt. of India, for awarding the BSR Faculty Fellowship No. F.18-1/2011(BSR), date: 07-03-2019, and DST, CSIR, UGC, DRDO, and AICTE, Govt. of India, for the financial support in the form of major research project grants. H.T.D. thanks RUSA. The authors also acknowledge CIF, Pondicherry University, for providing the characterization facilities. T.M. acknowledges the financial support from the Scheme for Promotion of Academic and

Research Collaboration (SPARC) of the Ministry of Human Resource Development (MHRD), Government of India, SPARC Grant No. SPARC/2018-2019/P1122/SL.

■ REFERENCES

- (1) Grätzel, M. Dye-sensitized solar cells. *J. Photochem. Photobiol., C* **2003**, *4*, 145–153.
- (2) Kakiage, K.; Aoyama, Y.; Yano, T.; Oya, K.; Fujisawa, J. I.; Hanaya, M. Highly-efficient dye-sensitized solar cells with collaborative sensitization by silyl-anchor and carboxy-anchor dyes. *Chem. Commun.* **2015**, *51*, 15894–15897.
- (3) Stephan, A. M. Review on gel polymer electrolytes for lithium batteries. *Eur. Polym. J.* **2006**, *42*, 21–42.
- (4) Balaji, T. E.; Tanaya Das, H.; Maiyalagan, T. Recent trends in Bimetallic Oxides and their composites as electrode materials for Supercapacitor applications. *ChemElectroChem* **2021**, *8*, 1723–1746.
- (5) Chandra, A.; Chandra, A.; Thakur, K. Synthesis, characterization and polymer battery fabrication of hot-pressed ion conducting nanocomposite polymer electrolytes. *Composites, Part B* **2014**, *60*, 292–296.
- (6) Tanaya Das, H.; Mahendrababu, K.; Maiyalagan, T.; Elumalai, P. Performance of solid-state hybrid energy-storage device using reduced graphene-oxide anchored sol-gel derived Ni/NiO nanocomposite. *Sci. Rep.* **2017**, *7*, No. 15342.
- (7) Sun, K.-C.; Arbab, A.-A.; Sahito, I.-A.; Qadir, M.-B.; Choi, B.-J.; Kwon, S.-C.; Yeo, S.-Y.; Yi, S.-C.; Jeong, S.-H. A pvdf-based electrolyte membrane for a carbon counter electrode in dye-sensitized solar cells. *RSC Adv.* **2017**, *7*, 20908–20918.
- (8) Wang, Z.; Lin, Z.; Deng, J.; Shen, S.; Meng, F.; Zhang, J.; Zhang, Q.; Zhong, W.; Gu, L. Elevating the d-Band center of six-coordinated octahedrons in Co₉S₈ through Fe-incorporated topochemical deintercalation. *Adv. Energy Mater.* **2021**, *11*, No. 2003023.
- (9) Vinoth, S.; Kanimozhi, G.; Prasad, K. H.; Kumar, H.; Srinadhu, E.; Satyanarayana, N. Enhanced ionic conductivity of electrospun nanocomposite (pvdf-hfp/TiO₂ nanofibers fillers) polymer fibrous membrane electrolyte for DSSC application. *Polym. Compos.* **2019**, *40*, 1585–1594.
- (10) Barbosa, J.-C.; Dias, J. P.; Lanceros-Mendez, S.; Costa, C.-M. Recent advances in poly(vinylidene fluoride) and its copolymers for lithium-ion battery separators. *Membranes* **2018**, *8*, No. 45.
- (11) Vijayakumar, E.; Subramania, S.; Fei, Z.; Dyson, P. J. High performance dye sensitized solar cell based on electrospun poly(vinylidene fluoride-co-hexafluoropropylene)/Cobalt sulfide nanocomposite membrane electrolyte. *RSC Adv.* **2015**, *5*, 52026–52032.
- (12) Bandara, T. M. W. J.; Fernando, H. D. N. S.; Furlani, M.; Albinsson, I.; Dissanayake, M. A. K. L.; Mellander, B.-E. Performance enhancers for gel polymer electrolytes based on LiI and RbI for quasi-solid-state dye sensitized solar cells. *RSC Adv.* **2016**, *6*, 103683–103691.
- (13) Lee, J.-Y.; Bhattacharya, B.; Kim, D.-W.; Park, J.-K. Poly(ethylene oxide)/poly(dimethylsiloxane) blend solid polymer electrolyte and its dye-sensitized solar cell applications. *J. Phys. Chem. C* **2008**, *112*, 12576–12582.
- (14) Kanimozhi, G.; Vinoth, S.; Kumar, H.; Srinadhu, E.-S.; Satyanarayana, N. Conductivity and dielectric permittivity studies of KI based nanocomposite (PEO/PMMA/KI/I₂/ZnO nanorods) solid polymer electrolytes. *Polym. Compos.* **2019**, *40*, 2919–2928.
- (15) Lee, Y.-L.; Shen, Y.-J.; Yang, Y.-M. A hybrid pvdf-hfp/nanoparticle gel electrolyte for dye-sensitized solar cell applications. *Nanotechnology* **2008**, *19*, No. 455201.
- (16) Feng, Yu.; Li, W.; Yafei, H.; Yu, Y.; Cao, W. P.; Zhang, T.; Fei, W. Enhanced dielectric properties of PVDF-HFP/BaTiO₃-nanowires composites induced by interfacial polarization and wire-shape. *J. Mater. Chem. C* **2015**, *3*, 1250–1260.
- (17) Leones, R.; Costa, C.-M.; Machado, A.-V.; Esperana, J.-M.-S. S.; Silva, M.-M.; Lanceros-Mendez, S. Effect of ionic liquid anion type in the performance of solid polymer electrolytes based on poly-

- (vinylidene fluoride-trifluoroethylene). *Electroanalysis* **2015**, *27*, 457–464.
- (18) Senthil, R.; Theerthagiri, J.; Madhavan, J.; Ganesan, S.; Arof, A. Influence of organic additive to PVDF-HFP mixed iodide electrolytes on the photovoltaic performance of dye-sensitized solar cells. *J. Phys. Chem. Solids* **2017**, *101*, 18–24.
- (19) Nunes-Pereira, J.; Lopes, A. C.; Costa, C. M.; Leones, R.; Silva, M. M.; Lanceros-Mendez, S. Porous membranes of montmorillonite/poly(vinylidene fluoride-trifluoroethylene) for Li-ion battery separators. *Electroanalysis* **2012**, *24*, 2147–2156.
- (20) Ahmed, S.; Rafat, M.; Singh, M. K.; Hashmi, S.-A. A free-standing, flexible PEDOT:PSS film and its nanocomposites with graphene nanoplatelets as electrodes for quasi-solid-state supercapacitors. *Nanotechnology* **2018**, *29*, No. 395401.
- (21) Vinoth, S.; Hariprasad, K.; Kanimozhi, G.; Satyanarayana, N. Electrospun nanocomposite polymer fibrous membrane electrolyte for DSSC. *AIP Conf. Proc.* **2005**, No. 070008.
- (22) Kumar, P.; Singh, A.; Kumar, V.; Kundu, P. Incorporation of nano-Al₂O₃ within the blend of sulfonated-PVdF-co-HFP and nafion for high temperature application in DMFC. *RSC Adv.* **2015**, *5*, 63465–63474.
- (23) Kanimozhi, G.; Vinoth, S.; Kumar, H.; Srinadhu, E.-S.; Satyanarayana, N. A novel electrospun cobalt-doped zinc oxide nanofibers as photoanode for dye-sensitized solar cell. *Mater. Res. Express* **2019**, *6*, No. 025041.
- (24) Kanimozhi, G.; Vinoth, S.; Kumar, H.; Srinadhu, E. S.; Satyanarayana, N. Electrospun Nanocomposite Ag–ZnO Nanofibrous Photoanode for Better Performance of Dye-Sensitized Solar Cells. *J. Electron. Mater.* **2019**, *48*, 4389–4399.
- (25) Yu, L.; Skov, A. ZnO as a cheap and effective filler for high breakdown strength elastomers. *RSC Adv.* **2017**, *7*, 45784–45791.
- (26) Vinoth, S.; Kanimozhi, G.; Kumar, H.; Srinadhu, E.-S.; Satyanarayana, N. High conducting nanocomposite electrospun PVDF/HFP/TiO₂ quasi-solid electrolyte for dye-sensitized solar cell. *J. Mater. Sci.: Mater. Electron.* **2018**, *30*, 1199–1213.
- (27) Zhang, J.; Han, H.; Wu, S.; Xu, S.; Zhou, C.; Yang, Y.; Zhao, X. Ultrasonic irradiation to modify the PEO/P(VdF-HFP)/TiO₂ nanoparticle composite polymer electrolyte for dye sensitized solar cells. *Nanotechnology* **2007**, *18*, No. 295606.
- (28) Senthil Kumar, P.; Sakunthala, A.; Govindan, K.; Reddy, M. V.; Prabu, M. Single crystalline TiO₂ nanorods as effective fillers for lithium ion conducting PVdF-HFP based composite polymer electrolytes. *RSC Adv.* **2016**, *6*, 91711–91719.
- (29) Lee, Y.-S.; Shin, W.-K.; Kim, J.; Kim, D.-W. High performance composite polymer electrolytes for lithium-ion polymer cells composed of a graphite negative electrode and LiFePO₄ positive electrode. *RSC Adv.* **2015**, *5*, 18359–18366.
- (30) Zhang, J.; Yang, Y.; Wu, S.; Xu, S.; Zhou, C.; Hu, H.; Chen, B.; Xiong, X.; Sebo, B.; Han, H.; Zhao, X. End-functional silicone coupling agent modified PEO/P(VdF-HFP)/SiO₂ nanocomposite polymer DSSC. *Nanotechnology* **2008**, *19*, No. 245202.
- (31) Zhu, Y.; Cao, J.; Chen, H.; Qipeng, Y.; Li, B. High Electrochemical Stability of 3D cross-linked network PEO@nano-SiO₂ composite polymer electrolyte for Lithium metal batteries. *J. Mater. Chem. A* **2019**, *7*, 6832–6839.
- (32) Kaur, J.; Lee, J.; Shofner, M. Influence of polymer matrix crystallinity on nanocomposite morphology and properties. *Polymer* **2011**, *52*, 4337–4344.
- (33) Šupová, M.; Martynková, G. S.; Barabaszová, K. Effect of nanofillers dispersion in polymer matrices: A Review. *Sci. Adv. Mater.* **2011**, *3*, 1–25.
- (34) Fu, S.-Y.; Sun, Z.; Huang, P.; Li, Y.; Hu, N. Some basic aspects of polymer nanocomposites: A critical review. *Nano Mater. Sci.* **2019**, *1*, 2–30.
- (35) Vinoth, S.; Kanimozhi, G.; Narsimulu, D.; Kumar, H.; Srinadhu, E. S.; Satyanarayana, N. Ionic relaxation of electrospun nanocomposite polymer-blend quasi-solid electrolyte for high photovoltaic performance of Dye-sensitized solar cells. *Mater. Chem. Phys.* **2020**, *250*, No. 122945.
- (36) Gao, R.; Wang, L.; Geng, Y.; Ma, B.; Zhu, Y.; Dong, H.; Qiu, Y. Effects of an intercalation nanocomposite at the photoanode/electrolyte interface in quasi-solid dye-sensitized solar cells. *J. Phys. Chem. C* **2011**, *115*, 17986–17992.
- (37) Vickraman, P.; Senthilkumar, V. A study on the role of BaTiO₃ in Lithiumbis(perfluoroethanesulfonyl)imide-based PVDF-HFP nanocomposites. *Ionics* **2010**, *16*, 763–768.
- (38) Wu, N.; Cao, Q.; Wang, X.; Li, S.; Li, X.; Deng, H. In situ ceramic fillers of electrospun thermoplastic polyurethane/poly(vinylidene fluoride) based gel polymer electrolytes for Li-ion batteries. *J. Power Sources* **2011**, *196*, 9751–9756.
- (39) Liao, L.; Lien, C. F.; Shieh, D. L.; Chen, F. C.; Lin, J. L. FTIR study of adsorption and photochemistry of amide on powdered TiO₂: Comparison of benzamide with acetamide. *Phys. Chem. Chem. Phys.* **2002**, *4*, 4584–4589.
- (40) Pavlova-Verevkin, O. B.; Ozerina, L. A.; Politova, E. D.; Surin, N. M.; Ozerin, A. N. Effect of electrolytes on the slow aggregation of TiO₂ nanocrystals. *Colloid J.* **2009**, *71*, 529–533.
- (41) Popov, I.; Nigmatullin, R.; Koroleva, E.; Nabereznov, A. The generalized Jonscher's relationship for conductivity and its confirmation for porous structures. *J. Non-Cryst. Solids* **2012**, *358*, 1–7.
- (42) Pike, G. E. AC conductivity of scandium oxide and a new hopping model for conductivity. *Phys. Rev. B* **1972**, *6*, 1572–1580.
- (43) Dyre, J. C. The random free-energy barrier model for ac conduction in disordered solids. *J. Appl. Phys.* **1988**, *64*, 2456–2468.
- (44) Funke, K.; Banhatti, R.; Grabowski, P.; Nowinski, J.; Wrobel, W.; Dinnebier, R.; Magdysyuk, O. Low-temperature α -AgI confined in glass: Structure and dynamics. *Solid State Ionics* **2015**, *271*, 2–9.
- (45) Funke, K.; Wilmer, D. Concept of mismatch and relaxation derived from conductivity spectra of solid electrolytes. *Solid State Ionics* **2000**, *136–137*, 1329–1333.
- (46) Funke, K. Jump relaxation in solid electrolytes. *Prog. Solid State Chem.* **1993**, *22*, 111–195.
- (47) Daz, E. G.; Gonzalez, E.; Garcia, M. F.; Asensio, I. A. Kinetic study of the pyrolysis of canary pine: The relationship between the elemental composition and the kinetic parameters. *Ind. Eng. Chem. Res.* **2018**, *57*, 9094–9101.
- (48) Havriliak, S.; Negami, S. A complex plane representation of dielectric and mechanical relaxation processes in some polymers. *Polymer* **1967**, *8*, 161–210.
- (49) Iacob, C.; Sangoro, J. R.; Serghei, A.; Naumov, S.; Korth, Y.; Krger, J.; Friedrich, C.; Kremer, F. Charge transport and glassy dynamics in imidazole-based liquids. *J. Chem. Phys.* **2008**, *129*, No. 234511.
- (50) Kanimozhi, G.; Kumar, H. Modeling of solar cell under different conditions by ant lion optimizer with lambertw function. *Appl. Soft Comput.* **2018**, *71*, 141–151.
- (51) Kanimozhi, G.; Rajathy, R.; Kumar, H. Minimizing energy of point charges on a sphere using symbiotic organisms search algorithm. *Int. J. Electr. Eng. Inf.* **2016**, *8*, 29–44.
- (52) Vinoth, S.; Kanimozhi, G.; Kumar, H.; Srinadhu, E.-S.; Satyanarayana, N. Symbiotic organism search algorithm for simulation of j-v characteristics and optimizing internal parameters of dssc developed using electrospun TiO₂ nanofibers. *J. Nanopart. Res.* **2017**, *19*, No. 388.
- (53) Yang, Y.; Zhang, J.; Zhou, C.; Wu, S.; Xu, S.; Liu, W.; Han, H.; Chen, B.; Zhao, X. Effect of lithium iodide addition on poly(ethylene oxide)-poly(vinylidene fluoride) polymer-blend electrolyte for dye-sensitized nanocrystalline solar cell. *J. Phys. Chem. B* **2008**, *112*, 6594–6602.